# A new proposal for the reaction mechanism of light-dependent protochlorophyllide oxidoreductase

Pedro J. Silva[1,2] and Qi Cheng[3,4]

[1]FP-I3ID/Fac. de Ciências da Saúde, Universidade Fernando Pessoa, Porto, Portugal

[2]UCIBIO@REQUIMTE, BioSIM, Departamento de Biomedicina, Faculdade de Medicina, Universidade do Porto, Porto, Portugal

[3]College of Life Sciences, Hebei Agricultural University, Baoding, Hebei, 071000, China

[4]State Key Laboratory of North China Crop Improvement and Regulation, Hebei Agricultural University, Baoding, Hebei, 071000, China cheng.qi@heqishi.com

## Abstract

The light-dependent protochlorophyllide oxidoreductase is one of the few known enzymes that require a quantum of light to start their catalytic cycle. Upon excitation, it uses NADPH to reduce the $C_{17}$-$C_{18}$ in its substrate (protochlorophyllide) through a complex mechanism which has heretofore eluded precise determination. Isotopic-labelling experiments have shown that the hydride transfer step is very fast, with a small barrier close to 9 kcal·mol$^{-1}$, and is followed by a proton-transfer step , which has been postulated to be the protonation of the product by the strictly conserved Tyr189 residue. Since the structure of the enzyme-substrate complex has not been determined experimentally yet, we first used modelling techniques to discover the actual substrate binding mode. Two possible binding modes were found, both yielding stable binding (as ascertained through molecular dynamics simulations) but only one of which placed

the critical C17=C18 bond consistently close to the NADPH p*ro-S* hydrogen and to Tyr189. This binding pose was then used as starting point for the testing of the previous mechanistic proposals using time-dependent density functional theory. The quantum-chemical computations clearly showed that such mechanisms have prohibitively high activation energies. Instead, these computations showed the feasibility of a new mechanism begun by excited-state electron transfer from the key Tyr189 to the substrate: this process dramatically increases the acidity of Tyr189, which immediately transfers its proton (through an intervening water molecule) to the substrate $C_{18.}$ The electron hole left at Tyr189 is filled by an electron released from the strictly conserved Cys222, and hydride transfer from NADPH proceeds with a predicted barrier fully compatible with the experimental data. The reactions ends when the extra electron is returned to Cys222. This mechanism appears to agree with the extant experimental data, and re-interprets the final protonation step as a proton transfer to the active site itself, aimed at regenerating it for a new round of catalysis.

## Introduction

In all photosynthetic organisms, chlorophylls function as light-absorbing photo-pigments harvesting a range of light energy with various wavelengths. Chlorophyll biosynthesis recurs in similar ways in anoxygenic phototrophic proteobacteria as well as oxygenic phototrophic cyanobacteria, algae and higher plants[1–4]. In this pathway (chlorophyll biosynthesis), the two-electron reduction of the C17-C18 double bond in protochlorophyllide to chlorophyllide is a key step. Two distinctive versions of protochlorophyllide oxidoreductase (POR) enzymes are present in most photosynthetic organisms: a light-dependent version known as LPOR (absent, however, from

anoxygenic photosynthetic bacteria) and a light-independent version known as "dark-operative POR", or DPOR (which is absent from angiosperms). These two enzymes are structurally and genetically different, and their evolutionary stories are fascinating[2,5–10]. Phylogenetic analysis shows that LPOR first arose in cyanobacteria probably under strong evolutionary pressures to find an oxygen-insensitive enzyme capable of effecting PChlide reduction[2,9]. The gene was inherited by land plants from cyanobacteria ancestors, and now LPOR is the only PChlide reductase in angiosperms. LPOR belongs to the short-chain dehydrogenase/reductase superfamily whereas DPOR is, surprisingly, genetically and evolutionarily related to nitrogenase, a multi-subunit metalloenzyme capable of converting atmospheric nitrogen into ammonia, whereas. Despite relatively low identity at the aminoacid level, the crystal structures of both nitrogenase[11–14] and DPOR[15,16], not only share overall structure similarities but also interact with related Fe-S proteins which act as their electron-donors upon ATP hydrolysis[17,18]. Although extensive research on LPOR and DPOR has been carried out at the molecular levels over the past two decades[2,19,28–35,20–27] the precise details of their mechanisms still remain insufficiently described. It is generally assumed that LPOR uses light absorbed by its substrate PChlide in coordinating with its co-factor NADPH for hydride transfer from *pro*-S face of the nicotinamide ring to the $C_{17}$ position of the PChlide molecule, followed by a proton transfer reaction taken place from a conserved Tyr residue to the $C_{18}$ position of PChlide. Catalysis by LPOR is also thought to involve thermally excited protein dynamics that allow molecular motions occur on an ultrafast timescale[36], which makes it unique from other members of short-chain dehydrogenase super-family. Structural studies have until recently been restricted to the insights obtained from homology modeling[37–39], but the publication of the first X-ray crystal structures of LPOR from both model cyanobacteria *Synechocystis sp.PCC 6803* and

*Thermosynechococcus elongatus* complexed with cofactor NADPH[40] now allows a more well-grounded investigation of the precise molecular determinants of ligand binding and catalysis. However, unlike the DPOR-PChlide complex, the precise PChlide-binding site in LPOR-NADPH complex is yet to be determined. In this manuscript, we describe the computational discovery of a promising binding mode, which we used as starting point for a quantum-mechanical exploration of the reaction mechanism. We expect the insights obtained from this research to offer fruitful venues for further mechanistic investigations and eventual adaptation of the LPOR framework to non-natural catalysis.

**Computational methods**

Docking and molecular dynamics were performed in YASARA[41]. Substrate parameterization was performed with the AM1BCC protocol[42,43]. All molecular dynamics simulations were run with the AMBER03 forcefield[44], using a multiple time step of 2.5 fs for intramolecular and 5 fs for intermolecular forces. Simulations were performed in cells 15 Å larger than the solute along each axis (final cell dimensions 83 × 79× 77 Å), and counter-ions (45 $Cl^-$ and 43 $Na^+$) were added to a final concentration of 0.9 % NaCl. In total, the simulations contained approximately 51,630 atoms. A 8 Å cut-off was taken for Lennard-Jones forces and the direct space portion of the electrostatic forces, which were calculated using the Particle Mesh Ewald method [45] with a grid spacing <1 Å, 4th order B-splines and a tolerance of $10^{-4}$ for the direct space sum. Simulated annealing minimizations started at 298 K, velocities were scaled down with 0.9 every ten steps for a total time of 5 ps. After annealing, simulations were run at 298 K. Temperature was adjusted using a Berendsen thermostat[46] based on the time-

averaged temperature, i.e., to minimize the impact of temperature control, velocities were rescaled only about every 100 simulation steps, whenever the average of the last 100 measured temperatures converged.

Since the available starting structure[40] of the light-dependent protochlorophyllide reductase from *Synechocystis* (PDB:6R48 , chain B) is in a closed conformation, PChlide was initially placed just outside the cleft lying between Ile153 and the 225-250 domain, oriented so that its C17 atom faced the NADPH *pro-S* hydrogen. The initial distance between these two atoms (which we joined with a spring with force constant 3 kcal·mol-1/Å$^2$) was 14.5 Å. PChlide was then brought closer to the *pro-S* hydrogen through an umbrella sampling simulation by progressively decreasing the equilibrium distance of the spring by 1 Å every 3 ns. The structure we obtained after the simulation was more open than the starting structure (partly through conformational unravelling of the 225-250 domain) but it still did not afford a good docking pose. We used this structure as target for docking after replacing the unwound 225-250 domain with its initial (properly folded) structure, while keeping it in the newly generated open orientation relative to the rest of the protein. Substrate docking was then performed with AutoDock Vina[47] using default docking parameters. The docking region was confined to a 29.0×29.0×29.0 Å box centered on the crevice revealed by the umbrella sampling simulation. The sidechains of the aminoacids lining the crevice (Leu149, Lys152, Ile155, Tyr189, Lys190, Lys193, Tyr219, Cys222, Thr226, Leu228, Phe229, Tyr233, Phe236, Thr248 and Lys249) were kept flexible. 100 docking runs were performed. The docking poses showing appropriate orientation and distances of the C17 and NADPH pro-S hydrogen atoms were then subjected to molecular dynamics simulations for at least 100 ns. In the initial 25 ns of each simulation the NADPH-C17 and Tyr219-C18

distances were progressively shortened to prevent the escape of the ligand from the active site cleft. All restraints were removed at timepoint 25.000 ns.

The stable structure obtained after 300 ns of MD simulation was used as the starting point for the computation of the potential of mean force for ligand binding. The potential of mean force was obtained through umbrella sampling simulations performed by constraining the distance between the ligand $Mg^{2+}$ atom and the Val14 amide nitrogen atom (which is located in the base of the identified pocket) with a harmonic potential of the form $V = 1/2k(x - x_0)^2$ with *k* equal to 14.0 kcal/mol/Å$^2$ . Sampling was performed in bins 0.7 Å apart, for 6 ns per bin. In each bin, the first full ns was discarded from the analysis. The unbiased distributions were obtained through the weighted histogram analysis method (WHAM)[48,49] using a bin size of 0.2 Å.

Density-functional and time-dependent density functional computations were performed using the PBE0 functional[50,51] ,which has been shown to provide good results when applied to the analysis of singlet, triplet, valence and Rydberg excited states in combination with large basis sets, returning a mean absolute error of 0.28 eV (the lowest among global hybrids tested) [52]. The size of our system prevents the use of such large basis sets, but preliminary computations with basis sets of different sizes showed that in our PChlide+NADPH+Tyr189 system the 6-31G(d) basis set yielded the same excitations as those obtained with a larger number of polarization functions and/or diffuse functions, and afforded excitation energies within 0.1 eV of the energies computed with those larger basis sets. All TDDFT computations and geometry optimizations were therefore performed with the 6-31G(d) basis set. Between eight and ten excited states were computed in each TDDFT run. Although TDDFT is known to under-estimate the energies of excitations with charge-transfer character, this limitation is not expected to qualitatively affect our results, since the relevant charge-transfer state

we detected (see below) geometrically relaxes into a deprotonated state without any energetic barrier: any effect of the under-estimation of the original excited state energy is therefore expected to, at most, provide an even more spontaneous relaxation into that state.

Due to the extremely high computational cost of DFT and TDDFT computations in large systems, we performed our computations in suitably truncated models with varying sizes. All models included the full protochlorophyllide (with the propionate group replaced by an ethyl substituent) and either the nicotinamide ring of NADPH or the complete sidechain of Tyr189. The model systems were saturated with hydrogen atoms, which replaced the NH-and C=O groups removed from Tyr189 and the O-ribosyl removed from NADPH. Several water molecules (either bridging the Tyr189 with $C_{18}$ or solvating the amide moiety of the nicotinamide) were also included. Larger models included both the nicotinamide ring and Tyr189. To prevent the truncation of the system from allowing unrealistic movements of the NADPH/Tyr189/PChlide moieties, several atoms were kept frozen during the optimizations: the central Mg, three atoms in the PChlide ring, the Cα and Cβ atoms of Tyr189, and the nicotinamide methyl carbon atom which connects to the rest of the NADPH molecule in the protein structure. Coordinates were taken from Autogenerated delocalized coordinates [53] were used for geometry optimizations. Transition-state structures from the ground-state potential energy surfaces were confirmed by checking that a single imaginary frequency was present, corresponding to a vibration connecting the reactant and product states. ZPVE and thermal effects were computed at 298.15 K using scaling factor of 0.9726 [54] for the computed vibrational frequencies. Single-point energies of the DFT-optimized geometries were then calculated using the same functional using the 6-311G(d,p) basis set, supplemented with diffuse functions on non-hydrogen atoms. Due to extensive

linear dependence, SCF convergence could only be reached after removal of the diffuse functions from the carbon atoms which were part of the porphyrin delocalized π-system. This basis set will be referred to herein as 6-311G(partial+)(d,p). For reactions in excited states, computational cost prevented us from computing exact transition states: in these cases, we built the corresponding potential energy surfaces (PES) by sequentially constraining the bond length of interest (in 0.10 Å increments), and performing full optimization subject to those constraints. Each PES contained a single maximum between the reactant and product state, which was selected as an appropriate approximation of the corresponding transition state. The excited-state-tracking feature present in Firefly was used to ensure that the correct excited state was kept when constraining the reaction coordinate to successively larger/smaller values. Activation energies of electron transfer between aminoacid sidechains and Tyr189/PChlide radicals were computed using a Marcus theory formalism[55]: briefly, the geometries of all species thought to be involved in one-electron transfer were separately optimized in both oxidation states, the electron-transfer reorganization energies were then computed by using the oxidized geometry for the reduced state (and vice-versa), and finally Marcus parabolas were built from these values to ascertain the energy at their intersection. The influence of the solvent and protein environment on the reorganization energy (the outer-shell reorganization energy), could not be evaluated due to the prohibitive computational cost. Our reorganization energies are therefore approximate, and cannot provide a precise quantitative estimate. Electron-transfer rates were computed as described by Moser and Dutton[56] using an adaptation of the equation $\log k_{ET} = 15.0 - 0.6R - 3.1\frac{(\Delta G + \lambda)^2}{\lambda}$, where R is the inter-center distance (in Å), ΔG is the change in energy between reactants and products (in eV) and λ is the reorganization

energy (in eV). The factor $\frac{(\Delta G+\lambda)^2}{4\lambda}$ corresponds to the activation energy of an electron-transfer where the reorganization energy of the product state is equal to the reorganization energy of the reactant state, and when it is replaced by the more accurate activation energy computed using the Marcus parabolas built using the different reorganization energies of each state (as described above), that expression becomes $\log k_{ET} = 15.0 - 0.6R - 12.4\Delta G_{act}$. All ground-state energy values described in the text include solvation effects (ε=10) computed using the Polarizable Continuum Model [57–59] implemented in Firefly. Quantum chemistry computations were performed with the Firefly [60] quantum chemistry package, which is partially based on the GAMESS (US) [61] source code.

To ascertain the relative abundance of the different protonation or redox states of the aminoacid sidechains of the enzyme, continuum electrostatic calculations were performed using MEAD[62] AMBER14 charges and radii[63] were assigned to the protein structure using YASARA. The solvent probe radius was 1.4 Å, which should provide a reasonable spherical approximation of the water molecule. The ionic exclusion layer thickness was set at 2.0 Å, and temperature at 300 K. The dielectric constant used for the solvent region was 80, the approximate value for bulk water at room temperatures. The dielectric constant for the protein interior was set to 15, the value previously found to yield optimum results with this method[64,65]. A two-step focusing method was used. A first calculation using a (300 Å)$^3$ cube with a 1.0-Å lattice spacing, centered on the protein was followed by a second calculation using a (75 Å)$^3$ cube with a 0.25-Å spacing, centered on the titrable site. All Asp, Glu, His, Cys, Tyr and Lys residues were allowed to titrate. The sampling of proton-binding states was done using the MCRP program (Monte Carlo for Reduction and Protonation), which implements a Monte Carlo method described by Baptista *et al.* [66]. Sampling was performed at 0.5 pH units

intervals in the 6 - 8 range using $10^7$ Monte Carlo steps. For redox titrations, deprotonated Tyr189 and deprotonated Cys222 were allowed to transition between their anionic and radical neutral forms. Sampling was performed from pH 6 to 8 at 0.4 pH unit intervals, and in a redox potential window 800 mV-wide, at 20 mV intervals, using $10^7$ Monte Carlo steps.

## Results

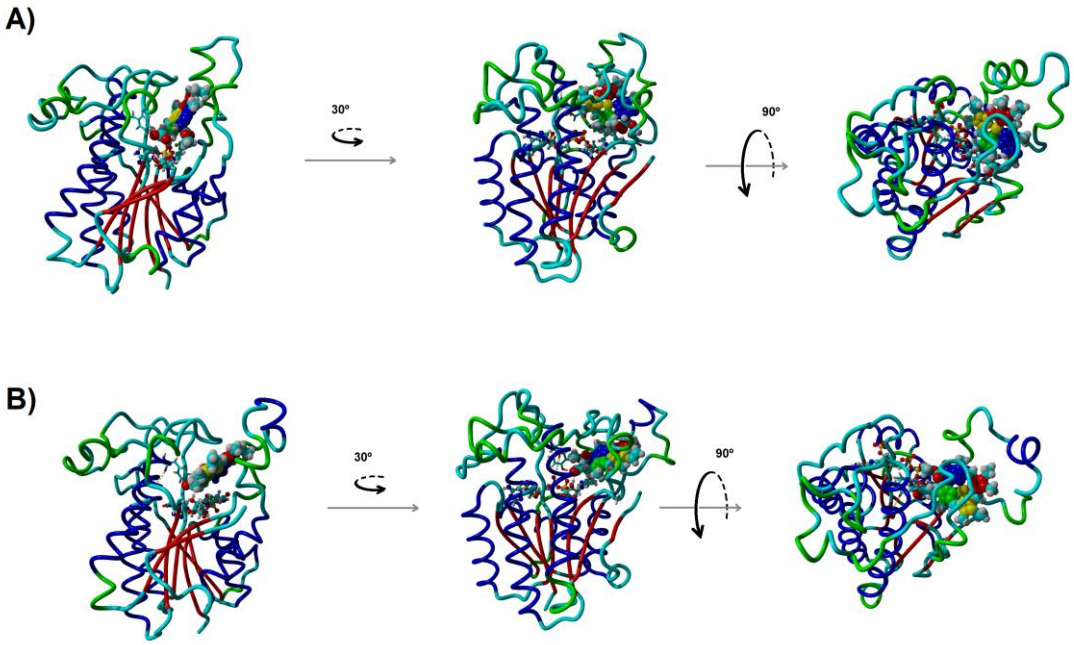


Figure 1: Comparison of the two binding modes of PChlide to LPOR. Both snapshots were taken 100 ns into each molecular dynamics simulation.A) Tyr189 close to the reactive ring D, propionic acid sidechain on ring D interacts with the backbone of Val142; B) Tyr189 interacts with the propionic acid sidechain on ring D. Rings are color-coded for ease of reference: yellow (ring A), red (ring B), blue (rings C and E) and green (ring D).

### *Identification of the substrate binding mode*

Molecular docking on the artificially-opened cavity obtained through steered molecular dynamics revealed two plausible binding modes with appropriate NADPH-C17 distances. In both cases, however, the reactive C=C bond remained relatively far

from the catalytically important Tyr189 and much closer to another tyrosine residue, Tyr219. Molecular dynamics simulations started from each of these positions converged into different conformations (Figure 1). The first pose (Figure 2) afforded a binding mode where one face of the protochlorophylide contacts the protein surface and the circumference of the substrate is almost completely accessible to the solvent. Portions of the flexible 225-250 domain partially shield the other face of the protochlorophyllide from the solvent: ring B is sandwiched between Pro154 and Leu228 and the ethyl substituent in its C8 atom lies in a pocket defined by Tyr233, Phe236 and Val247. The propionate group attached to protochlorophyllide C17 anchors the substrate in place through a strong interaction (2.11 ± 0.32 Å) with the amide nitrogen of Val142 and a short (3.00 ± 0.39 Å) C17-NADPH distance is maintained throughout. Tyr189 is properly placed in relative proximity (5.08 ± 0.92) Å to the protochlorophyllide C18 atom, separated from the C18 atom by a single water molecule which can act as a proton relay. Computation of the potential of mean force for this binding mode yielded a value of 26.1±0.7 kcal·mol$^{-1}$, far more favorable than the 8.4 kcal·mol$^{-1}$ computed for the binding mode computed by Zhang *et al.*[40]

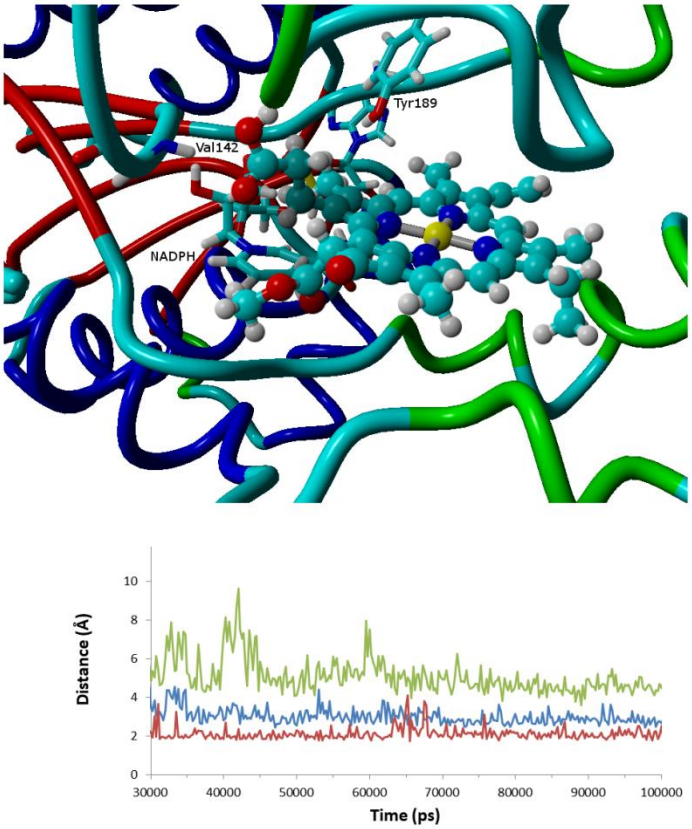


Figure 2: First stable binding pose. The graph depicts the time-evolution of NADPH-C17 (blue), Val142 NH-propionate (red) and Tyr189-C18 (green) distances.

In the second pose (Figure 3) anchoring of the substrate is performed instead through the interaction of the propionate group with Tyr189 (1.79 ± 0.32 Å) and the C2-hydroxyl group of the NADPH ribose (1.77 ± 0.20 Å). Compared to the first pose the lies 180º degrees flipped along the protochlophylide plane, so that, although ring B still lies in the pocket defined by the inner surface of the flexible 225-250 domain and ring D lies above the NADPH nicotinamide ring, ring A in the second pose roughly occupies the position taken up by rings C and E in the first pose and *vice versa*. The keto group in the E ring is markedly less exposed to the solvent in this conformation than in the previous pose. In this pose NADPH consistently remains farther from C17 (4.08 ± 0.48 Å) than in the previous conformation and no proton donor is ever present close to C18,

which strongly argues against a role for this conformation in the catalytic cycle. Quantum chemical computations on the reaction mechanism were therefore performed using the coordinates obtained from the simulation of the previous conformation. The snapshot taken at 100 ns was used for this purpose.

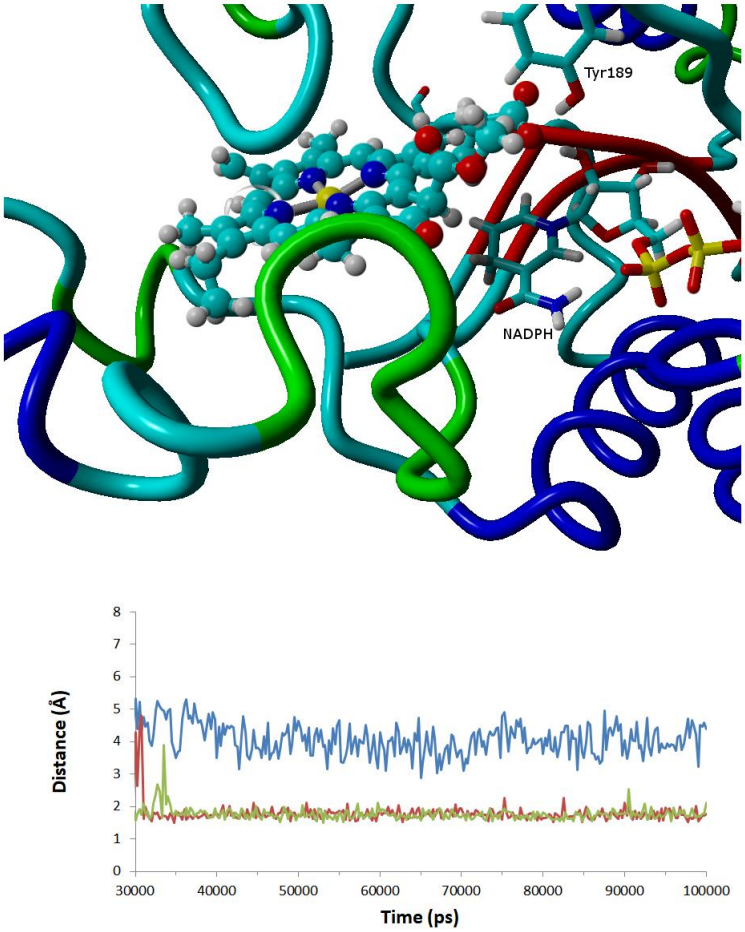


Figure 3: Second stable binding pose. The graph depicts the time-evolution of NADPH-C17 (blue), propionate-ribose (green) and Tyr189-propionate (red) distances.

285

***DFT exploration of the reaction mechanism arising from ground- or excited- state hydride transfer from NADPH to PChlide***

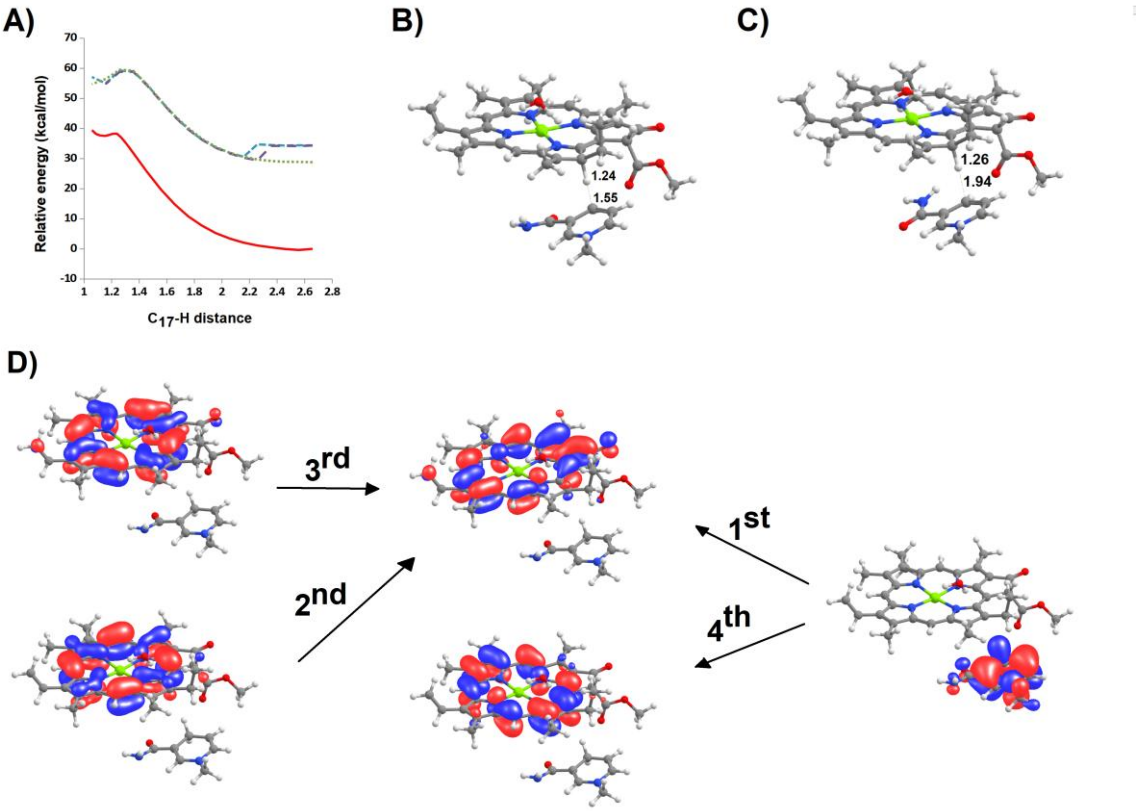


Figure 4: Hydride transfer from NADPH to PChlide. A) Potential energy surfaces at the ground-state (red) and the
290 first four excited states (green, blue and violet) B) Approximate structure of the transition state in the ground potentia energy surface. C) Approximate structure of the transition state in the first excited potentia energy surface. D) Orbitals involved in the first four excitations of the NADPH:PChlide system.

In agreement with previous computational studies[33,39], our new DFT computations
295 found that the activation energy of the ground-state hydride transfer from NADPH to protochlorophylide $C_{17}$ is prohibitively high, at 39.8 kcal·mol$^{-1}$ (Figure 4A). In the first four excited states this activation energy is lowered to 28.5 – 30.8 kcal·mol$^{-1}$, still well above the upper limit compatible with experimentally-detectable reaction rates (for example, Eyring's equation predicts that a reaction rate as low as 1 per hour requires an

activation energy below 22.3 kcal·mol$^{-1}$) and considerably above the 8.8 kcal·mol$^{-1}$ determined experimentally[33]. All excited-state potential energy surfaces are similar, and indeed the energies of the 3$^{rd}$ and 4$^{th}$ excited states become almost indistinguishable from those of the 1$^{st}$ and 2$^{nd}$ excited states when the distance between the NADPH hydride and the receiving $C_{17}$-atom in protochlorophyllide decreases below 2.1 Å. The geometries of the transition states in three out of four of these excited potential energy surfaces are quite similar to each other, with the hydride much closer (1.25 Å) to the receiving $C_{17}$ than to the donating nicotinamide $C_4$ atom (1.95 Å), whereas in the remaining excited potential surface (the 2$^{nd}$ one) the nicotinamide ring is significantly closer to PChlide and the hydride is much closer to the midpoint of those two atoms (1.35 Å from $C_{17}$ and 1.4 Å from the nicotinamide $C_4$ atom). This difference is not, however, especially interesting, since in all four excited potential energy surfaces the energies of these two structures are remarkably similar (< 0.5 kcal/mol), and therefore the region around the transition state is quite flat. The return of the hydride to NADP$^+$ is extremely fast, with activation energies below 2 kcal·mol$^{-1}$ in the ground state, and below 5 kcal·mol$^{-1}$ in any of the four excited states. In this mechanism, the transferred hydride will therefore promptly return to NADP$^+$ unless the formed PChlide:H$^-$ intermediate immediately acquires a proton, thereby yielding a stable Chlide. DFT study of that step clearly shows, however, that proton transfer from Tyr189 to the PChlide:H$^-$ (Figure 5B-D) is not as fast as required: the computed activation energy for the water-assisted transfer of that proton (7.6 kcal·mol$^{-1}$) yields a reaction rate $10^2$ – $10^4$ times slower than that of the return of the hydride to NADP$^+$. Both the extremely high endergonicity of the hydride transfer and the difficulty in protonating the PChlide:H$^-$ intermediate before the hydride returns to NADP$^+$ very strongly suggest that the actual reaction mechanism should not proceed as a two-step process initiated by hydride

transfer, but rather as either a concerted process or a two-step process initiated by proton- or single-electron-transfer.

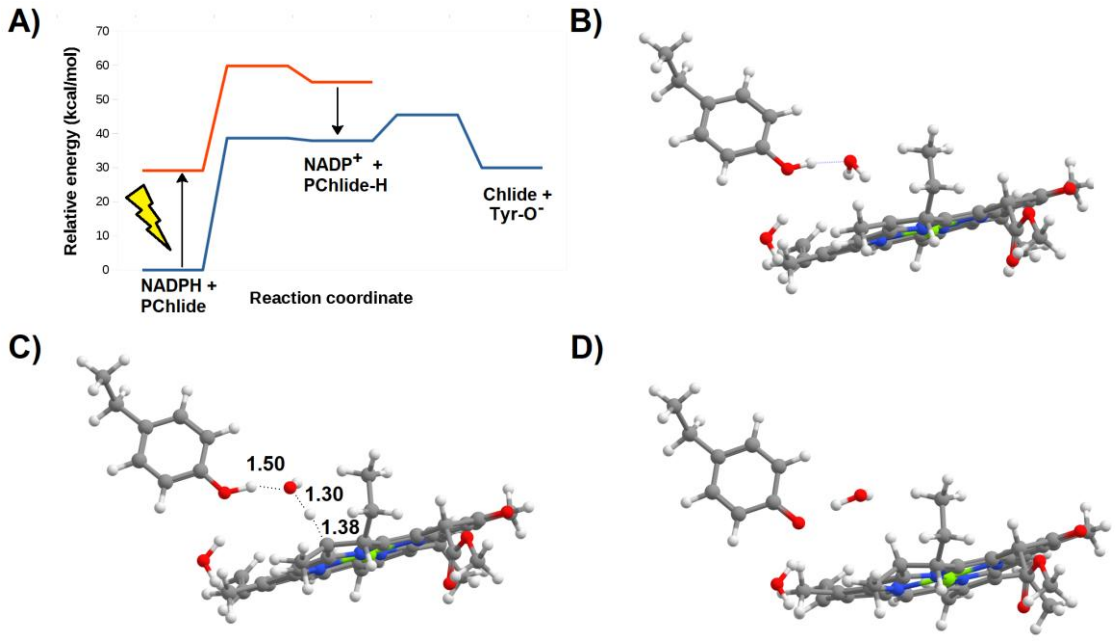


Figure 5: Potential energy surface in the pathway beginning with excited-state hydride transfer from NADPH to PChlide. A) Relative reaction energies of the intervening intermediates and transition states. B) Reactant state in the Tyr189:PChlide-hydride proton transfer step. C) Transition state of the proton transfer step from Tyr189 to the hydride-reduced PChlide. D) Final state of the proton-transfer state. All distances in ångstrom.

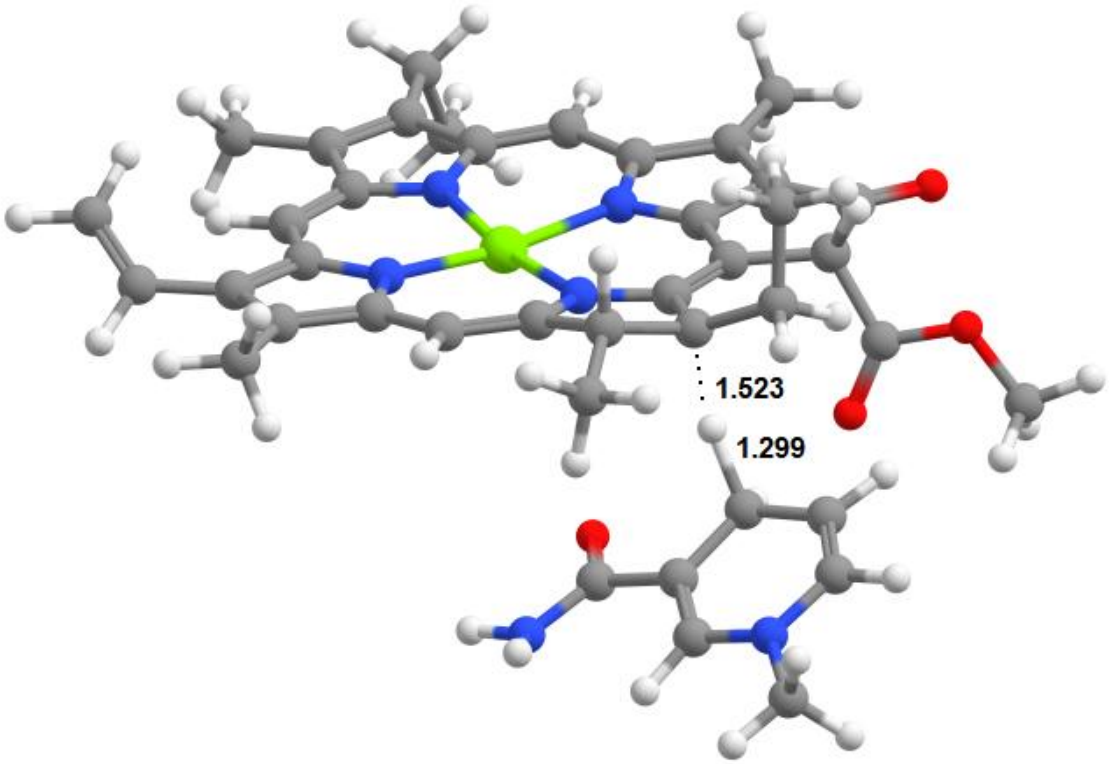


Figure 6: Transition state of the hydride transfer from NADPH to C18-protonated PChlide. Distances in ångstrom.

Such pathways are, however, not possible in the ground state. A two-step process initiated by proton transfer to $C_{18}$ cannot occur because, although subsequent hydride transfer from NADPH to a $C_{18}$-protonated PChlide (Figure 6) proceeds extremely fast (with activation energies ranging between 1 kcal·mol$^{-1}$ (B3LYP/6-311G(+)(d,p)//B3LYP/6-31G(d) [19]) and 3.2 kcal·mol$^{-1}$(PBE0/6-311(partial+)G(d,p)//PBE0/6-31G(d) [this work]) the initial protonation of PChlide at the $C_{18}$ position by Tyr189 is inaccessible in the ground state because it lies 45.3 kcal·mol$^{-1}$ above the neutral Tyr189:PChlide system. Addition of seven water molecules to the model system to facilitate charge delocalization can only reduce the endergonicity of this proton-transfer step to 37.1 kcal·mol$^{-1}$, which clearly establishes that this reaction is impossible in the ground state (Figure 7). On the other hand, simultaneous hydride

transfer from NADPH to $C_{17}$ and proton-transfer from Tyr189 to $C_{18}$ was also shown by our computations to be unfeasible in the ground state, due to an extremely high activation energy of 56.0 kcal·mol$^{-1}$. The reaction is endergonic by 26.2 kcal·mol$^{-1}$. This value entails that the oxidation of the chlorophyllide product by $NADP^+$ (with concurrent return of the $C_{18}$ proton to Tyr189) will have a high activation energy (56.0-26.2=29.8 kcal·mol$^{-1}$), which explains why the protein:Chlide:$NADP^+$ formed in the end of the catalytic cycle does not decay back into reactants in spite of the thermodynamic spontaneity of the reverse reaction.

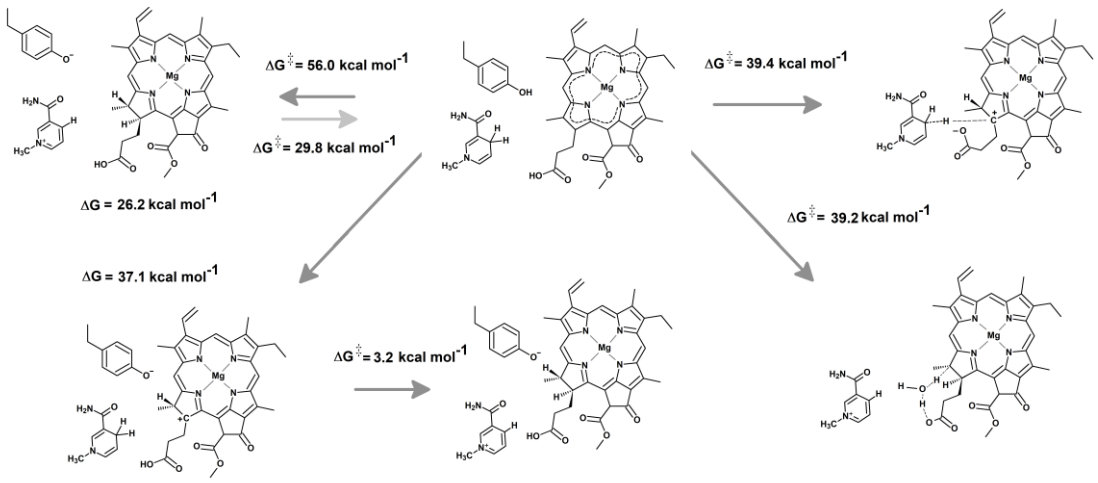


Figure 7: Analysis of the thermodynamic and kinetic feasibility of different ground state mechanisms.

Alternative protonation of the critical $C_{17}$=$C_{18}$ bond by a putative protonated form of the propionic acid substituent present in the $C_{17}$ position of PChlide also proved unfeasible, in spite of the higher acidity of the carboxylic acid: earlier computations[19] had already shown that in the absence of explicit water molecules this proton transfer is slow and thermodynamically disfavored (activation energy of 24.7 kcal·mol$^{-1}$ and endergonicity 19.8 kcal·mol$^{-1}$), and our new computations showed that expansion of that computational model with additional water molecules created a water chain that further facilitated the return of the proton in $C_{18}$ to the propionate. The $C_{18}$-protonated intermediate was therefore no longer stable, and only concerted proton/hydride transfer

mechanisms could occur. Two-dimensional scans of the potential energy surface detected two saddle points, corresponding to two distinct partially concerted mechanisms. In one of the saddle points, located 39.2 kcal·mol$^{-1}$ above the initial NADPH:Chlide-COOH state, hydride transfer is almost complete (the $C_{17}$-hydride bond is 1.14 Å long) and the incoming proton (provided by a water molecule which has just abstracted a proton from the propionic acid) still lies 1.48 Å away from $C_{18}$. In the other saddle point, which lies 39.4 kcal·mol$^{-1}$ above the reactants, the proton donated to $C_{18}$ lies only 1.13 Å away, whereas the hydride lies 1.34 Å from $C_{17}$ and 1.45 Å away from the nicotinamide. Not surprisingly, transferring a proton from the propionic acid to the PChlide:H$^-$ (whether this molecule has been generated in the ground state or through an excitation) yields a lower barrier than that arising from proton transfer from Tyr189 to PChlide:H$^-$, but is still unable to yield a mechanism compatible with the experimental observations due to the high activation energy of the hydride transfer from NADPH to PChlide. Finally, one-electron transfer from NADPH to PChlide is also impossible in the ground state, due to the 48.4 kcal·mol$^{-1}$ difference in NADPH ionization energy and PChlide electron affinity.

***DFT exploration of novel reaction pathways***

Our time-dependent DFT computations on the NADPH/substrate system described above showed that, although PChlide-centered charge-separated states are indeed low-lying (as the second and third excited states), subsequent hydrogen transfer is prohibitively expensive, since it proceeds with an activation energy of 28-30 kcal·mol$^{-1}$, far in excess of the experimentally computed barrier[33] of 8.8 kcal·mol$^{-1}$. We therefore turned our attention to the analysis of a mechanism starting from an initial light-induced

electron-transfer from NADPH to the protochlorophyllide, followed by proton transfer from the $NADPH^+$ cation radical to the substrate anion radical, which has been proposed by Archipowa et al. to explain the transient absorption experimental data as arising from four individual electron (or proton) transfers[67]. Two excited states characterized by complete charge-transfer from NADPH to PChlide could indeed be found in our TD-DFT computations on the NADPH/PChlide system (Figure 4D). Exploration of these excited states potential energy surfaces on the larger NADPH/PChlide/Tyr189 system revealed that the transition state for the postulated transfer of the remaining $H^+$:$e^-$ from NADPH to the PChlide anion lies, like the transfers of the full hydride to the $\pi$ -$\pi^*$ excited PChlide described earlier, more than 25 kcal·$mol^{-1}$ above the excited-state-relaxed geometry of the $NADPH^+$:$PChlide^-$ ion pair, still far above the experimental activation energy. TD-DFT computations on this NADPH/PChlide/Tyr189 system revealed us the existence of two low-lying excited states characterized by a hitherto unsuspected excitation from an occupied $\pi$ orbital in Tyr189 into an unoccupied $\pi^*$ orbital in the PChlide substrate (Figure 8).

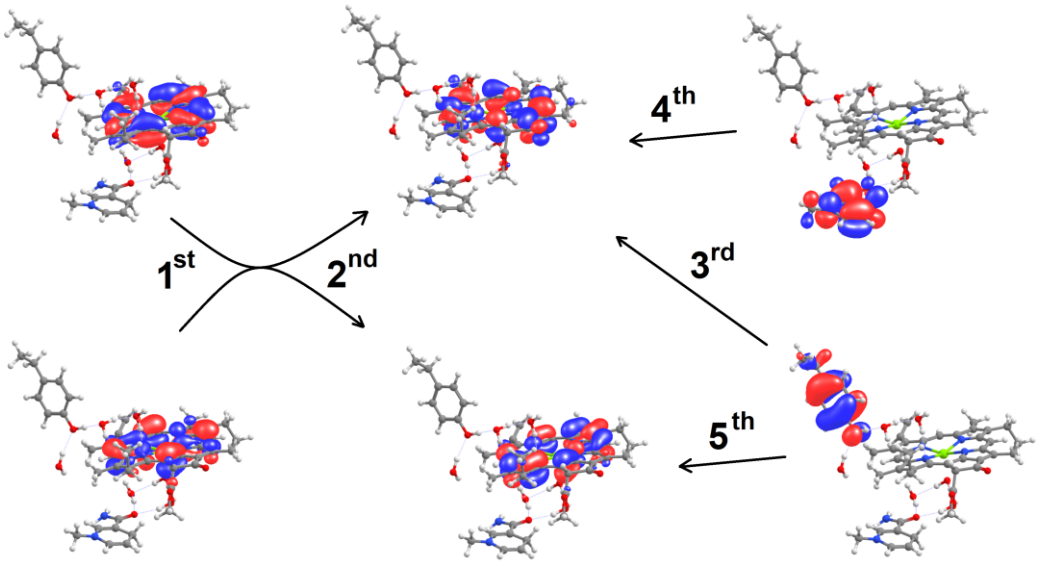


Figure 8: Orbitals involved in the five lowest-energy excitations in the NADPH/protochlorophyllide/Tyr189 system.

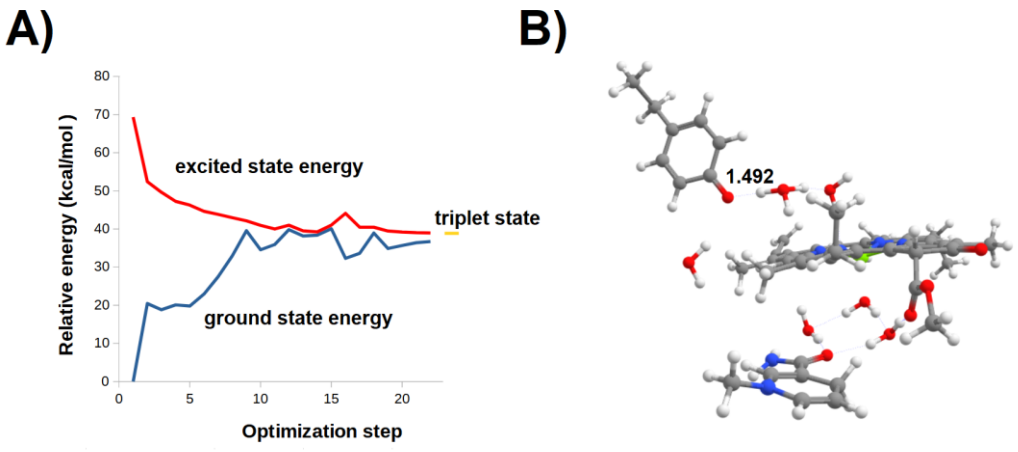


Figure 9: Evolution of the π Tyr189 – $\pi^*$ PChlide excited state upon geometry optimization. A) Excited- and ground-state energies of the system during geometry optimization; B) Optimized geometry of the final Tyr189·:PChlide$^-$:$H_3O^+$ system.

Optimization of this excited state showed spontaneous proton transfer from the one-electron-oxidized Tyr189 to the water molecule placed between this residue and the one-electron-reduced substrate (Figure 9B), yielding a neutral radical on the deprotonated Tyr189, a PChlide anion radical, and a $H_3O^+$ lying 2.15 Å from the substrate $C_{18}$. The electronic structure of this excited state is effectively an open-shell singlet with a S=½ electron in the substrate and a S=-½ electron on the Tyr189, and its optimized structure corresponds to a point in the potential energy surface where the excited and ground states almost intersect. Should the system relax into the ground state, its geometry would then spontaneously return to the initial state and the reaction would not proceed. Three different factors concur to prevent this relaxation: first, the oscillator strength of the transition to the ground state (as computed by TDDFT) is extremely small, which entails a very low probability of fluorescence; additionally, this excited state has almost exactly the same energy as the corresponding triplet state produced by inversion of the spin of the transferred electron (Figure 9A) , which entails that (if spin-orbit coupling in the PChlide$^-$ system is strong enough) the excited electron

may spontaneously change spin after moving to PChlide, thereby rendering its return to Tyr189 impossible due to Pauli's exclusion principle. Such a spin-flip of a putative internal charge-transfer state has indeed already been observed in both free protochlorophyllide and PChlide:LPOR:NADPH complex upon excitation with 450nm light[68]. Finally, even in the absence of such a spin-flip other aminoacids sidechains in the protein structure may be oxidized by the deprotonated Tyr189 radical, which would then increase the distance between the S= ½ and S=-½ electrons and prevent them from quickly recombining into the original electronic distribution.

We have therefore computed the oxidation potentials of tryptophane, phenylalanine, cysteine (neutral and deprotonated) and tyrosine (neutral and deprotonaded) sidechains. Electron transfer from deprotonated Cys to a deprotonated Tyr189 radical was shown by these computations to be consistently favorable (from -21 to -19 kcal·mol$^{-1}$ in the absence of explicit water molecules around Cys or Tyr, depending on the dielectric constant chosen for the medium, or -5.1 kcal·mol$^{-1}$ when water molecules are explicitly included around Tyr to mimic its solvent-exposed status, whereas Cys is kept unsolvated to simulate its less-exposed state), whereas no other alternative was found to afford spontaneous electron transfers at any dielectric constants. Electron-tunneling inside proteins is well-known to be feasible when the electron donors and acceptors are closer than 16 – 18 Å [69,70], and inspection of the three-dimensional structures of the enzyme from *Synechocystis* (PDB:6R48) and *Thermosynechococcus elongatus* (PDB:6RNW) showed the presence of three conserved cysteine residues 10.5 – 13 Å from Tyr189 (Cys85, Cys185 and Cys 222), as well as two conserved tyrosine residues in close proximity to Tyr189 (Tyr90, at 5 Å and Tyr219, 8 Å away) which we therefore suggest may be involved in the ultimate stabilization of the electron-separated state initially generated through the excitation of one Tyr189 electron into the substrate.

Computation of the activation energies of these electron-transfers (Table 1) reveals a negligible barrier of 0.1 kcal·mol$^{-1}$ for the electron transfer from bare deprotonated cysteine to microsolvated radical deprotonated tyrosine, which (combined with the crystallographic Cys-Tyr distances) translates[69] to an electron transfer rate of $10^{7.1}$ –$10^{8.6}$ s$^{-1}$. The electron transfer from the deprotonated forms of Tyr90 and Tyr219 to the radical deprotonated Tyr189 also has a very small activation energy (2.3 kcal·mol$^{-1}$), entailing a very fast rate of $10^{8.9}$ –$10^{9.5}$ s$^{-1}$.

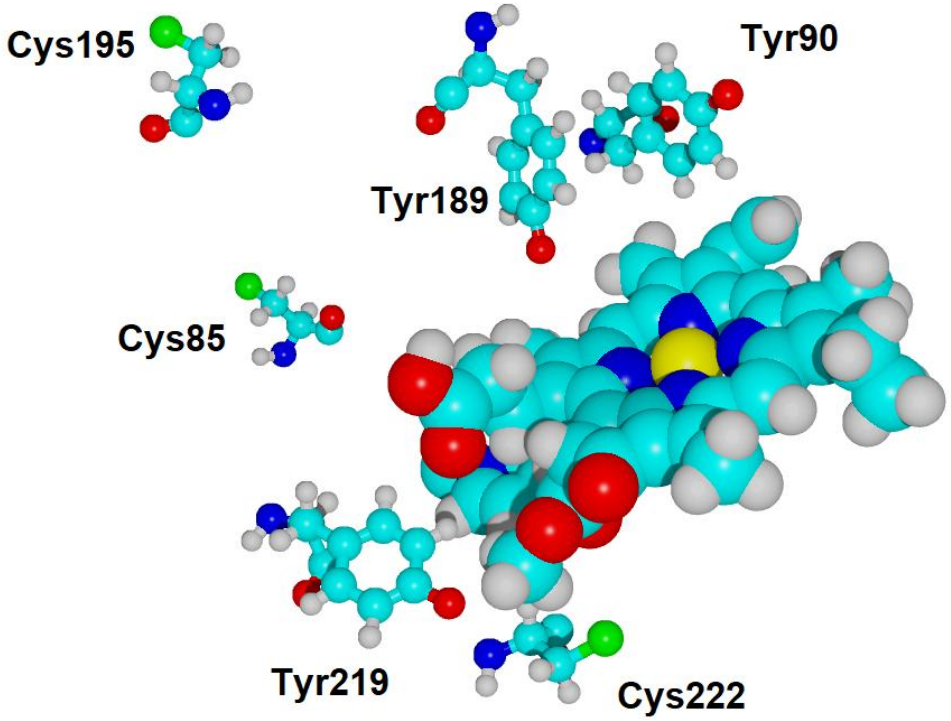


Figure 10: The geometric arrangement of substrate, Tyr189, and the five conserved Cys/Tyr residues present in its vicinity (as observed 100 ns throughout the MD simulation). Distances between sidechains remain stable from t=50 ns onwards. Although the simulation was run with the physiological protonation states, sidechains are depicted in their deprotonated forms, which are the ones susceptible to lose one electron to the deprotonated Tyr189 radical.

Table 1: Activation energies (in kcal·mol$^{-1}$) for the electron-transfers between unsolvated deprotonated Cys and different microsolvated tyrosine-based radicals. All values computed using a Marcus formalism using PBE0/6-311(partial+)G(d,p)//PBE0/6-31G(d). Solvation effects were included (ε=10).

| | | Electron-acceptor | | |
|---|---|---|---|---|
| | | Cys· | TyrOH·$^+$ | Tyr-O· |
| Electron donors | Cys$^-$ | 0.5 | 5.8 | 0.1 |
| | Tyr-OH | 45.8 | 4.2 | 41.9 |
| | Tyr-O$^-$ | 5.2 | 7.0 | 2.3 |

Table 2: Estimation of the "electron-hole" transfer velocities ($v_{ET}$) between Tyr189 and surrounding Tyr/Cys residues. $v_{ET}$ were computed by multiplying electron-transfer rates ($k_{ET}$, obtained through the Moser Dutton equation) by the amount of the reactive deprotonated form of the electron-donating aminoacid sidechain (computed through a Monte-Carlo procedure based on the results from continuum electrostatic calculations). All distances shown are the average values measured between t=100 ns and t=300 ns of our simulation. The geometric arrangement of these residues relative to the substrate is shown in Figure 10. The highest transfer velocities are highlighted in bold.

| Electron donor | Electron acceptor | distance (Å) | log $k_{ET}$ | relative abundance of the deprotonated form of the electron donor | log $v_{ET}$ |
|---|---|---|---|---|---|
| Tyr90 | Tyr189-O· | 3.9 ± 0.4 | 11.4 | $3.9\times10^{-3}$ | **9.0** |
| Tyr219 | Tyr189-O· | 9.0 ± 0.6 | 8.4 | $4.4\times10^{-3}$ | **6.0** |

| | | | | | |
|---|---|---|---|---|---|
| Cys85 | Tyr189-O· | 14.2 ± 0.6 | 6.4 | $1.5\times10^{-4}$ | 2.6 |
| Cys195 | Tyr189-O· | 11.9 ± 0.8 | 7.8 | $3.0\times10^{-5}$ | 3.3 |
| Cys222 | Tyr189-O· | 13.4 ± 1.0 | 6.9 | $1.6\times10^{-4}$ | 3.1 |
| Tyr189 | Tyr90-O· | 3.9 ± 0.4 | 11.4 | $2.3\times10^{-2}$ | **9.8** |
| Cys222 | Tyr90-O· | 16.2 ± 1.1 | 5.2 | $1.6\times10^{-4}$ | 1.4 |
| Tyr189 | Tyr219-O· | 9.0 ± 0.6 | 8.4 | $2.3\times10^{-2}$ | 6.7 |
| Cys222 | Tyr219-O· | 4.9 ± 0.6 | 12.0 | $1.6\times10^{-4}$ | **8.2** |

Table 2 details average distances between these sidechains and the estimated proportion (at pH=7.0) of the respective deprotonated forms, which are thermodynamically capable of reducing deprotonated Tyr189 radical. Application of the Moser-Dutton formula to these data shows that the "electron hole" in the deprotonated oxidized Tyr189 can very quickly transfer to either Tyr90 or Tyr219. Both Tyr90 and Tyr219 may quickly regain the electron they have released to Tyr189, but Tyr219 much more readily accepts it, instead, from Cys222. The spontaneity of this electron-transfer can be strongly increased by the protein environment: continuum electrostatics computations of the complete protein show that, even if the intrinsic redox potentials of deprotonated Tyr and deprotonated Cys were initially assumed to be the same (instead of favoring the deprotonated Cys radical by 5.1 $kcal\cdot mol^{-1}$, as in our quantum computations) the computed redox potential of the deprotonated Cys222 would be lowered by the protein environment by between 95 mv (at pH 8) and 110 mV (at pH 6) relative to that of the deprotonated Tyr189, which further confirms the high spontaneity of our proposed electron transfer from Cys222 to the deprotonated Tyr189 radical.

The migration of the electron-hole to Cys222 prevents the reaction from running backwards, since the extra electron now present in the PChlide can no longer return to Tyr189, which is occupied by the electron previously released by Tyr219/Cys222. Premature unproductive termination of the reaction through transfer of the extra electron from PChlide$^{-}$ to the oxidized Cys222·would be prevented both by the spin-flip described above (which would have aligned the spins in PChlide$^{-}$ and Cys222·) and by the presence of a Marcus inverted region caused by the high exergonicity of the putative electron transfer between both species (Figure 11 and Table 3).

This proposal is consistent with previous mutagenesis studies which showed that replacement of Cys222 by Ser[71] prevented the formation of the $A_{696}$ intermediate, decreased the reaction rate up to 15-fold, and greatly decreases the maximum amount of product generated. The observation of residual Chlide production in the mutant, where the characteristic 696 nm absorption of $A_{696}$ intermediate (known to be produced after subsequent hydride transfer) is not detected could then be explained by positing that this $A_{696}$ species does not simply correspond (as usually asumed) to the hydride reduced PChlide, but is instead due to the interaction of the one-electron-reduced PChlide with the radical form of the deprotonated Cys222·, whereas in the C222S mutant the radical electron-hole would remain in Tyr219 and not give rise to that absorption.

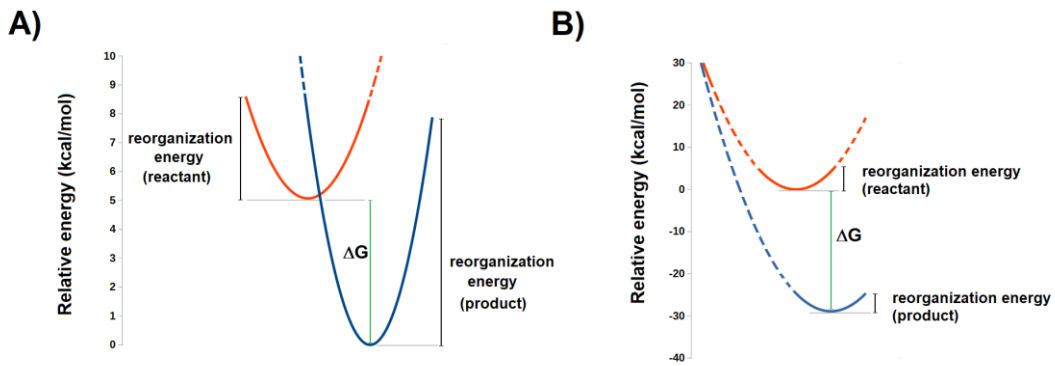


Figure 11: Marcus parabolas for the calculation of the activation energies of electron-transfers from: A) Cys$^{-}$ to the deprotonated neutral Tyr radical; B) PChlide$^{-}$ to deprotonated Cys· neutral

radical. The activation energy can be determined by comparing the initial state with the point where both parabolas intersect. A Marcus inverted region, where increased exergonicity leads to increased activation energies, is apparent in panel B due to the large value of the exergonicity relative to the respective reorganization energies.

We performed the study of the subsequent reactions in a truncated system missing the Tyr189 sidechain, both because of the extremely high likelihood of the transfer of the radical to Cys222 and because the computational exploration of potential energy surfaces in the excited state is extremely demanding, both in time and in computational resources, and fraught with difficulties. The electronic structure of this truncated S=½ system is much more amenable to SCF convergence than that of the open-shell excited state singlet, and the following steps can then be simulated as **ground state** proton transfer from the $H_3O^+$ generated in the previous step to the PChlide anion radical, followed by a hydride transfer to the $C_{18}$-protonated PChlide anion radical.

The decrease in system sized provided by the elimination of the Tyr189 residue afforded the opportunity to include a few extra water molecules to improve the description of the solvation of $H_3O^+$ while preserving computational tractability. In this improved system, we found that the separated $H_3O^+$ and one-electron-reduced substrate cannot coexist: instead, the substrate will become protonated either on its $C_{18}$ or $C_{20}$ atoms. The two states are connected by a transition state containing a Zundel-ion ($H_3O^+$:$H_2O$) hovering above the $C_{18}$ atom, 33.4 kcal·mol$^{-1}$ above the $C_{18}$-protonated product and 36.5 kcal·mol$^{-1}$ above the $C_{20}$-protonated alternative. These computations show that the proton may therefore spontaneously transfer to either $C_{18}$ or $C_{20}$, and is then kinetically trapped in that position. Although this truncated model is insufficient to explain why the $C_{18}$-product is always observed to be formed instead of the $C_{20}$-protonated alternative, we have noticed that the computation of the light-induced

deprotonation of Tyr189 is sensitive to the precise initial orientation of the Tyr189 and the positions of added waters, which can in some models yield an $H_3O^+$ hovering above $C_{18}$ and in others an $H_3O^+$ much closer to the $C_{20}$ atom. It is therefore likely that the precise reaction outcome is governed by dynamic factors that stabilize a Tyr189 orientation conducive to the formation of the $C_{18}$-product. An alternative mechanism involving direct hydride transfer from NADPH to the substrate anion radical **before** the proton transfer is impossible, as it is prevented by an activation energy of 35.9 kcal·mol$^{-1}$. The immediate product obtained after light-induced electron-transfer from Tyr189 to the substrate is therefore shown by these computations to be either a $C_{18}$-protonated or a $C_{20}$-protonated neutral PChlide radical (Figure 12). Interestingly, analysis of the reorganization energies in Tables 3 and 4 shows that premature radical quenching through electron transfer from the protonated $C_{18}$-protonated (or $C_{20}$-protonated) one-electron-reduced PChlide to the deprotonated Cys222 radical may be thermodynamically and kinetically possible, provided that the unpaired electrons in Cys222/protonated PChlide have opposite spins. Productive continuation of the reaction sequence therefore requires, as already hinted above, that the extra electron in the PChlide ring has undergone a spin-inversion.

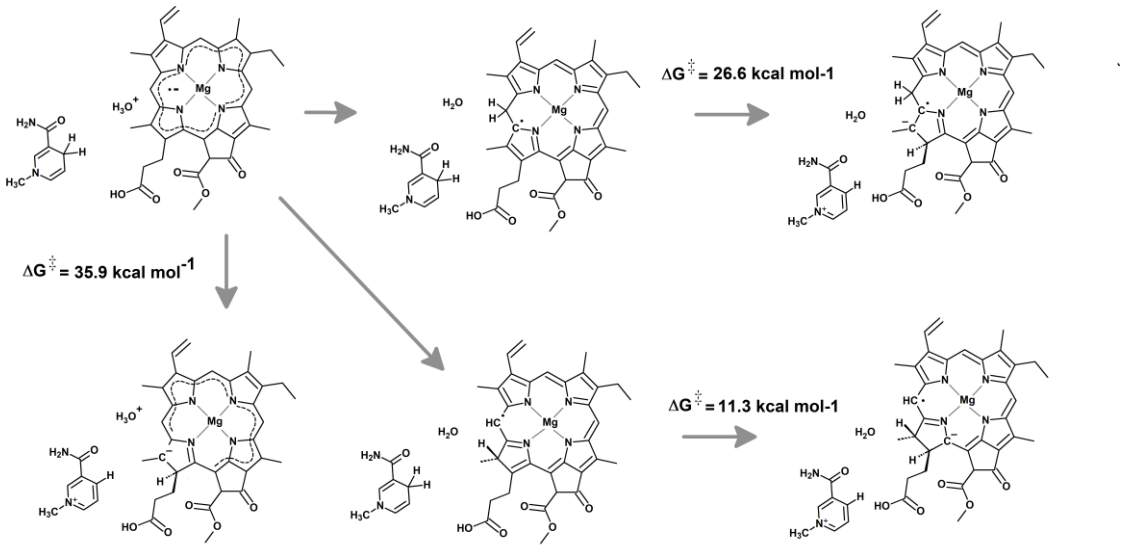


Figure 12: Possible reaction pathways of one-electron-reduced PChlide towards $H_3O^+$ and NADPH. The two protonation steps shown occur without a barrier.

Hydride transfer from NADPH to the putative $C_{20}$-protonated neutral radical is endergonic by 16.9 kcal·mol$^{-1}$ and has a high activation energy of 26.6 kcal·mol$^{-1}$. The $C_{20}$-protonated neutral radical intermediate therefore seems to be a kinetic dead end and, should the previous reaction step generate a $C_{20}$-protonated product, the reaction will not proceed further: at most, the proton will eventually return to Tyr189 when the extra electron present in the ring is recuperated by the Cys222 radical, yielding a futile cycle.

In contrast, hydride transfer from the NADPH to the $C_{18}$-protonated neutral radical is computed to be exergonic by 11.0 kcal·mol$^{-1}$ and to proceed very easily with a barrier of only 11.3 kcal·mol$^{-1}$, which agrees quite well with the 8.8 kcal·mol$^{-1}$ barrier determined experimentally[33] for the formation of the $A_{696}$ intermediate. Neither the differences in stability between the products or the activation energies of the reactions arising from hydride transfer to the $C_{18}$-protonated and $C_{20}$-protonated species are surprising, because in the latter instance the replacement of the $C_{16}$–$C_{17}$=$C_{18}$–$C_{19}$=$C_{20}$–$C_1$ conjugated segment by a non-conjugated ($C_{16}$–$C_{17}$–$C_{18}$=$C_{19}$–$C_{20}$–$C_1$) single bond breaks

the extended conjugated π-system, whereas converting only the $C_{17}$-$C_{18}$ double bond into a single bond has a much smaller effect on the length of the conjugated system. The product of this step is a one-electron reduced chlorophyllide, and the termination of the reaction will then proceed through the return of the extra electron to the deprotonated Cys222· radical. Tables 3 and 4 show that this quenching reaction has a very favorable activation energy (5.6 kcal·mol$^{-1}$) and is irreversible (due to the 35.7 kcal·mol$^{-1}$ barrier of the opposite reaction), and the short distance between Cys222 and the substrate (7.3 ± 0.6 Å) further facilitates its progress at very high rates, provided that a new spin-flip has occurred so that both electrons have opposite spins and that the reaction is, therefore, no longer spin-forbidden.

Experimental analysis of the "dark" steps following the hydride transfer has shown that at least two individual steps[72] are involved before the formation of the characteristic 671 nm absorption band attributed to the LPOR-NADP$^+$-Chlide ternary product complex, one of which is subject to a solvent isotope effect when the reaction is performed in deuterated water[33] and has been previoulsy attributed to proton transfer to hydride-reduced PChlide. In our model, the proton transfer takes place before the hydride transfer, and the observed solvent-isotope effect must therefore be attributed to a different event. We propose that this dependence is due, instead, to the uptake of a solvent proton by the deprotonated Cys222 after this sidechain has received the extra electron from Chlide$^-$ (and accompanying conformational change due to the change in charge distribution and flexibility of that region of the protein) to regenerate the active site for the next round of catalysis. In this interpretation, the intermediate (absorbing at 681 nm and fluorescing at 684 nm[72]), observed between the $A_{696}$ intermediate and the $A_{671}$ product would be a LPOR-NADP$^+$-Chlide ternary complex bearing an anionic Cys222, and the $A_{671}$ product would be the LPOR-NADP$^+$-Chlide ternary complex

bearing a neutral Cys222. This is consistent both with the a lack of solvent-isotope effect in the Cys222Ser mutant[71] and with the observation of significant influence of solvent viscosity for these steps (i.e. conformational changes), which (due to the close proximity of Tyr189 to solvent and substrate throughout our molecular dynamics model of the ternary complex) would be hard to explain in a model attributing this step to proton transfer from Tyr189 to substrate.

Table 3: Activation energies (in kcal·mol$^{-1}$) for the electron-transfers from one-electron-reduced (proto)chlorophyllide species to Cys- or Tyr-based radicals. All values computed using a Marcus formalism using PBE0/6-311(partial+)G(d,p)//PBE0/6-31G(d). Solvation effects were included (ε=10).

| Electron donor | Electron-acceptor | | |
|---|---|---|---|
| | Cys-S· | Tyr-OH·$^{+}$ | Tyr-O· |
| one-electron-reduced PChlide | 35.7 | 19.0 | 5.5 |
| C18-protonated one-electron-reduced PChlide | 0.3 | 4.8 | <0.1 |
| C20-protonated one-electron-reduced PChlide | <0.1 | 4.6 | <0.1 |
| one-electron-reduced Chlide | 5.6 | 12.6 | 2.6 |

Table 4: Activation energies (in kcal·mol$^{-1}$) for the electron-transfers from Cys or Tyr sidechains to neutral or cationic (proto)chlorophyllide species. All values computed using a Marcus formalism using PBE0/6-311(partial+)G(d,p)//PBE0/6-31G(d). Solvation effects were included (ε=10).

| | Electron-acceptor | | | |
|---|---|---|---|---|
| | PChlide | C18- | C20- | Chlide |

| | | | protonated PChlide | protonated PChlide | |
|---|---|---|---|---|---|
| Electron donors | Cys-S$^-$ | 64.6 | 2.1 | 4.0 | 35.7 |
| | Tyr-OH | 88.0 | 46.6 | 48.6 | 82.7 |
| | Tyr-O$^-$ | 39.5 | 6.9 | 9.1 | 37.7 |

## Discussion

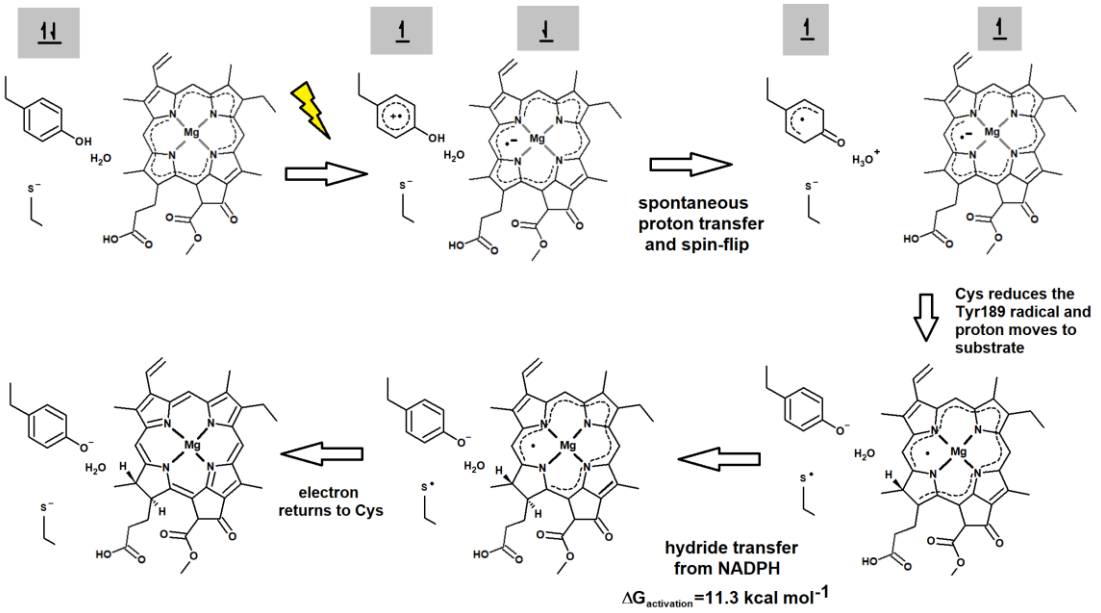


Figure 13: Proposed reaction mechanism. Spin orientation in the initial reaction stages is depicted in the grey boxes

The pathway (Figure 13) described above is very different from previous proposals[73], which generally start with either an initial hydride transfer from NADPH to excited substrate[67,68] or a single electron transfer from NADPH to substrate[71]. It is not, however, devoid of experimental support, since early electron-spin resonance studies of this reaction[74,75] mechanism reported the observation of radical signals identical to the ones generated upon chemical reduction of protochlorophyllide to its anion radical state.

Similar signals have, in other studies[29], been attributed to PChlide-based radical cations. The peak-to-peak linewidth of radical signals has been claimed to be sufficiently different to tell radical cation EPR signals from radical anions in chlorophyll[76] but small linewidths (usually attributed to the radical cations) have also been found in Mg-porphyrins in their radical anion state[77]. The precise attribution of the radical signals observed in the light-dependent protochlorophyllide reductase, their possible roles in the mechanism, and whether they are indeed, as suggested by our computations, due to one-electron reduced PChlide, one-electron-reduced Chlide or one-electron-reduced $C_{18}$-protonated PChlide must therefore await further experimental examination. The postulated one-electron-reduced forms of PChlide present in our mechanism also suggest the possibility of further side-reactions with possible biological consequences, since the excess of electronic charge in their extended conjugated systems increases their susceptibility to oxidation[78]. According to our computations of activation energies for the hydride transfer and electron-transfer steps, the one-electron $C_{18}$-protonated PChlide has the longest half-life (due to its activation energy of 11.3 kcal·mol$^{-1}$), whereas the one-electron reduced PChlide reacts with $H_3O^+$ without a barrier and the one-electron-reduced Chlide formed after hydride transfer must face a 5.6 kcal·mol$^{-1}$ barrier to return its extra electron to Cys222. We have therefore computed the activation energies of the electron-transfer reactions from these species to $O_2$, to ascertain the likelihood of any of them generating superoxide, thereby terminating the reaction mechanism (Table 5). Electron-transfer from the critical $C_{18}$-protonated PChlide intermediate is thermodynamically and kinetically disfavored, whereas both Chlide$^-$ and PChlide$^-$ are prone to donate an electron to $O_2$. In spite of the very small activation energies of these latter processes, we expect net superoxide production and premature reaction termination to be residual, due to the barrier-less reaction of PChlide$^-$ towards

$H_3O^+$, which leads to its unavailability to react with oxygen, and to the almost barrier-less activation energy for a subsequent electron-transfer from any superoxide (generated from $Chlide^-$) to the Cys222 radical.

Table 5: Activation energies (in $kcal \cdot mol^{-1}$) for the electron-transfers between oxygen and one-electron reduced species. All values computed using a Marcus formalism using PBE0/6-311(partial+)G(d,p)//PBE0/6-31G(d). Solvation effects were included (ε=10).

| **Electron-donor** | Electron-acceptor | Activation energy ( $kcal \cdot mol^{-1}$) |
|---|---|---|
| $PChlide^-$ | $O_2$ | 0.4 |
| $C_{18}$-protonated $PChlide^-$ | $O_2$ | 9.2 |
| Chlide- | $O_2$ | 0.2 |
| $O_2^-$ | PChlide | 18.7 |
| $O_2^-$ | $C_{18}$-protonated PChlide | 0.4 |
| $O_2^-$ | Chlide | 19.7 |
| $O_2^-$ | Cys-S· | <0.1 |

## Conclusions

In a previous work[39] (using smaller models and lacking excite-state geometry optimizations), we reported high barriers to the hydride-transfer step from NADPH to PChlide, although it went unnoticed at the time that those barriers were incompatible with the experimentally-measured barrier of 8.8 $kcal \cdot mol^{-1}$. The present work clearly establishes that such a hydride transfer is not feasible either on the ground state or in the excited state, and also ruled out the possibility of a sequential electron/hydrogen/proton

transfer begun through light-induced one-electron oxidation of NADPH by PChlide. In alternative, the computations described herein suggest a light-induced electron transfer from Tyr189 to PChlide, which strongly increases the acidity of Tyr189 and enables the transfer of a proton to the $C_{18}$ (or $C_{20}$) position of PChlide. The electron hole generated in Tyr189 quickly transfers to the strictly-conserved Cys222 through the (also completely conserved) Tyr219 residue, after which the "back-reaction" can no longer take place. Hydride transfer from NADPH to the $C_{17}$ position then takes place (with a computed barrier quite close to the experimental one), followed by return of the extra electron in the substrate to the deprotonated Cys222 radical, followed by the re-protonation of this residue by bulk solvent. A spin-flip of the extra-electron transferred from Tyr189 to PChlide prevents unproductive futile cycling from prematurely terminating the reaction. Beyond its excellent agreement with the experimentally-measured activation energy, this new model also appears to be consistent with a wide variety of experimental observations which have heretofore been interpreted in a different way, and suggests new experimental tests for the detection of the new postulated intermediates in this intriguing enzyme.

**Acknowledgments**

The computational resources used in this work have been acquired under project PTDC/QUI-QUI/111288/2009 (which was financed by FEDER through Programa Operacional Factores de Competitividade–COMPETE and by Portuguese Funds through FCT–Fundação para a Ciência e a Tecnologia). This work was also supported by the Applied Molecular Biosciences Unit–UCIBIO, which is financed by national funds from FCT (UIDB/04378/2020), by China Ministry of Science and Technology project no. 2019YFA0904701, and Qi's Academy.

References

(1) Gabruk, M.; Mysliwa-Kurdziel, B. Light-Dependent Protochlorophyllide Oxidoreductase: Phylogeny, Regulation, and Catalytic Properties. *Biochemistry* **2015**. https://doi.org/10.1021/acs.biochem.5b00704.

(2) Yang, J.; Cheng, Q. Origin and Evolution of the Light-Dependent Protochlorophyllide Oxidoreductase (LPOR) Genes. *Plant Biol.* **2004**. https://doi.org/10.1055/s-2004-821270.

(3) Willows, R. D. Biosynthesis of Chlorophylls from Protoporphyrin IX. *Nat. Prod. Rep.* **2003**, *20* (3), 327. https://doi.org/10.1039/b110549n.

(4) Masuda, T.; Fujita, Y. Regulation and Evolution of Chlorophyll Metabolism. *Photochem. Photobiol. Sci.* **2008**, *7* (10), 1131–1149. https://doi.org/10.1039/b807210h.

(5) Cheng, Q. Perspectives in Biological Nitrogen Fixation Research. *Journal of Integrative Plant Biology*. 2008. https://doi.org/10.1111/j.1744-7909.2008.00700.x.

(6) Cheng, Q.; Day, A.; Dowson-Day, M.; Shen, G. F.; Dixon, R. The Klebsiella Pneumoniae Nitrogenase Fe Protein Gene (NifH) Functionally Substitutes for the ChlL Gene in Chlamydomonas Reinhardtii. *Biochem. Biophys. Res. Commun.* **2005**. https://doi.org/10.1016/j.bbrc.2005.02.064.

(7) Suzuki, J. Y.; Bauer, C. E. A Prokaryotic Origin for Light-Dependent Chlorophyll Biosynthesis of Plants. *Proc. Natl. Acad. Sci. U. S. A.* **1995**, *92* (9), 3749–3753. https://doi.org/10.1073/pnas.92.9.3749.

(8) Fujita, Y.; Bauer, C. E. A Nitrogenase-Like Enzyme Catalyzing a Key Reaction for Greening in the Dark. In *The Porphyrin Handbook: Chlorophylls And Bilins: Biosynthesis, Synthesis And Degradation*; Kadish, K. M., Smith, K. M., Guilard, R., Eds.; Academic Press, 2003; Vol. 13, pp 109–156.

(9) Vedalankar, P.; Tripathy, B. C. Evolution of Light-Independent Protochlorophyllide Oxidoreductase. *Protoplasma* **2019**, *256* (2), 293–312. https://doi.org/10.1007/s00709-018-1317-y.

(10) Masuda, T.; Takamiya, K.-I. Novel Insights into the Enzymology, Regulation and Physiological Functions of Light-Dependent Protochlorophyllide Oxidoreductase in Angiosperms. *Photosynth. Res.* **2004**, *81* (1), 1–29. https://doi.org/10.1023/B:PRES.0000028392.80354.7c.

(11) Georgiadis, M. M.; Komiya, H.; Chakrabarti, P.; Woo, D.; Kornuc, J. J.; Rees, D. C. Crystallographic Structure of the Nitrogenase Iron Protein from Azotobacter Vinelandii. *Science* ***1992,*** *257,* 1653-1659. https://doi.org/10.1126/science.1529353.

(12) Kim, J.; Rees, D. C. Structural Models for the Metal Centers in the Nitrogenase Molybdenum-Iron Protein. *Science* **1992,** *257*, 1677-1682 , https://doi.org/10.1126/science.1529354.

(13) Schindelin, H.; Kisker, C.; Schlessman, J. L.; Howard, J. B.; Rees, D. C. Structure of ADP·AlF4/--Stabilized Nitrogenase Complex and Its Implications for Signal Transduction. *Nature* **1997,** *387*, 370-376, https://doi.org/10.1038/387370a0.

(14) Kim, J.; Rees, D. C. Crystallographic Structure and Functional Implications of the Nitrogenase Molybdenum–Iron Protein from Azotobacter Vinelandii. *Nature* **1992**, *360* (6404), 553–560. https://doi.org/10.1038/360553a0.

(15) Muraki, N.; Nomata, J.; Ebata, K.; Mizoguchi, T.; Shiba, T.; Tamiaki, H.; Kurisu, G.; Fujita, Y. X-Ray Crystal Structure of the Light-Independent Protochlorophyllide Reductase. *Nature* **2010**, *465* (7294), 110–114. https://doi.org/10.1038/nature08950.

(16) Bröcker, M. J.; Schomburg, S.; Heinz, D. W.; Jahn, D.; Schubert, W. D.; Moser, J. Crystal Structure of the Nitrogenase-like Dark Operative Protochlorophyllide

Oxidoreductase Catalytic Complex (ChlN/ChlB)2. *J. Biol. Chem.* **2010**, *285* (35), 27336–27345. https://doi.org/10.1074/jbc.M110.126698.

(17) Bröcker, M. J.; Virus, S.; Ganskow, S.; Heathcote, P.; Heinz, D. W.; Schubert, W.; Jahn, D.; Moser, J.; Bro, M. J. ATP-Driven Reduction by Dark-Operative Protochlorophyllide Oxidoreductase from Chlorobium Tepidum Mechanistically Resembles Nitrogenase Catalysis. *J. Biol. Chem.* **2008**, *283* (16), 10559–10567. https://doi.org/10.1074/jbc.M708010200.

(18) Bröcker, M. J.; Wätzlich, D.; Saggu, M.; Lendzian, F.; Moser, J.; Jahn, D. Biosynthesis of (Bacterio)Chlorophylls: ATP-Dependent Transient Subunit Interaction and Electron Transfer of Dark Operative Protochlorophyllide Oxidoreductase. *J. Biol. Chem.* **2010**. https://doi.org/10.1074/jbc.M109.087874.

(19) Silva, P. J. With or without Light: Comparing the Reaction Mechanism of Dark-Operative Protochlorophyllide Oxidoreductase with the Energetic Requirements of the Light-Dependent Protochlorophyllide Oxidoreductase. *PeerJ* **2014**, *2*, e551. https://doi.org/10.7717/peerj.551.

(20) Heyes, D. J.; Hunter, C. N. Making Light Work of Enzyme Catalysis: Protochlorophyllide Oxidoreductase. *Trends in Biochemical Sciences*. 2005. https://doi.org/10.1016/j.tibs.2005.09.001.

(21) Sytina, O. A.; Heyes, D. J.; Hunter, C. N.; Groot, M. L. Ultrafast Catalytic Processes and Conformational Changes in the Light-Driven Enzyme Protochlorophyllide Oxidoreductase (POR). *Biochem. Soc. Trans.* **2009**. https://doi.org/10.1042/BST0370387.

(22) Heyes, D. J.; Levy, C.; Sakuma, M.; Robertson, D. L.; Scrutton, N. S. A Twin-Track Approach Has Optimized Proton and Hydride Transfer by Dynamically Coupled

Tunneling during the Evolution of Protochlorophyllide Oxidoreductase. *J. Biol. Chem.* **2011**, *286* (13), 11849–11854. https://doi.org/10.1074/jbc.M111.219626.

(23) Hanf, R.; Fey, S.; Schmitt, M.; Hermann, G.; Dietzek, B.; Popp, J. Catalytic Efficiency of a Photoenzyme-An Adaptation to Natural Light Conditions. *ChemPhysChem* **2012**, *13* (8), 2013–2015. https://doi.org/10.1002/cphc.201200194.

(24) Zhong, D. Ultrafast Catalytic Processes in Enzymes. *Current Opinion in Chemical Biology*. 2007. https://doi.org/10.1016/j.cbpa.2007.02.034.

(25) Dietzek, B.; Tschierlei, S.; Hermann, G.; Yartsev, A.; Pascher, T.; Sundström, V.; Schmitt, M.; Popp, J. Protochlorophyllide a: A Comprehensive Photophysical Picture. *Chemphyschem* **2009**, *10* (1), 144–150. https://doi.org/10.1002/cphc.200800536.

(26) Dietzek, B.; Tschierlei, S.; Hanf, R.; Seidel, S.; Yartsev, A.; Schmitt, M.; Hermann, G.; Popp, J. Dynamics of Charge Separation in the Excited-State Chemistry of Protochlorophyllide. *Chem. Phys. Lett.* **2010**. https://doi.org/10.1016/j.cplett.2010.04.027.

(27) Sytina, O. A.; Van Stokkum, I. H. M.; Heyes, D. J.; Hunter, N. C.; Van Grondelle, R.; Groot, M. L. Protochlorophyllide Excited-State Dynamics in Organic Solvents Studied by Time-Resolved Visible and Mid-Infrared Spectroscopy. *J. Phys. Chem. B* **2010**. https://doi.org/10.1021/jp9089326.

(28) Heyes, D. J.; Kruk, J.; Hunter, C. N. Spectroscopic and Kinetic Characterization of the Light-Dependent Enzyme Protochlorophyllide Oxidoreductase (POR) Using Monovinyl and Divinyl Substrates. *Biochem. J.* **2006**, *394* (Pt 1), 243–248. https://doi.org/10.1042/BJ20051635.

(29) Heyes, D. J.; Heathcote, P.; Rigby, S. E. J.; Palacios, M. a; van Grondelle, R.; Hunter, C. N. The First Catalytic Step of the Light-Driven Enzyme Protochlorophyllide

Oxidoreductase Proceeds via a Charge Transfer Complex. *J. Biol. Chem.* **2006**, *281* (37), 26847–26853. https://doi.org/10.1074/jbc.M602943200.

(30) Heyes, D. J.; Sakuma, M.; Scrutton, N. S. Laser Excitation Studies of the Product Release Steps in the Catalytic Cycle of the Light-Driven Enzyme, Protochlorophyllide Oxidoreductase. *J. Biol. Chem.* **2007**, *282* (44), 32015–32020. https://doi.org/10.1074/jbc.M706098200.

(31) Heyes, D. J.; Menon, B. R. K. K.; Sakuma, M.; Scrutton, N. S.; Oxidoreductase, P. Conformational Events during Ternary Enzyme-Substrate Complex Formation Are Rate Limiting in the Catalytic Cycle of the Light-Driven Enzyme Protochlorophyllide Oxidoreductase. *Biochemistry* **2008**, *47* (41), 10991–10998. https://doi.org/10.1021/bi801521c.

(32) Heyes, D. J.; Sakuma, M.; Scrutton, N. S. Solvent-Slaved Protein Motions Accompany Proton but Not Hydride Tunneling in Light-Activated Protochlorophyllide Oxidoreductase. *Angew. Chem. Int. Ed. Engl.* **2009**, *48* (21), 3850–3853. https://doi.org/10.1002/anie.200900086.

(33) Heyes, D. J.; Sakuma, M.; de Visser, S. P.; Scrutton, N. S. Nuclear Quantum Tunneling in the Light-Activated Enzyme Protochlorophyllide Oxidoreductase. *J. Biol. Chem.* **2009**, *284* (6), 3762–3767. https://doi.org/10.1074/jbc.M808548200.

(34) Heyes, D. J.; Hardman, S. J. O.; Mansell, D.; Gardiner, J. M.; Scrutton, N. S. Mechanistic Reappraisal of Early Stage Photochemistry in the Light-Driven Enzyme Protochlorophyllide Oxidoreductase. *PLoS One* **2012**. https://doi.org/10.1371/journal.pone.0045642.

(35) Fujita, Y.; Bauer, C. E. Reconstitution of Light-Independent Protochlorophyllide Reductase from Purified Bchl and BchN-BchB Subunits. In Vitro Confirmation of

Nitrogenase-like Features of a Bacteriochlorophyll Biosynthesis Enzyme. *J. Biol. Chem.* **2000**, *275* (31), 23583–23588. https://doi.org/10.1074/jbc.M002904200.

(36) Heyes, D. J.; Hunter, C. N.; van Stokkum, I. H. M.; van Grondelle, R.; Groot, M. L. Ultrafast Enzymatic Reaction Dynamics in Protochlorophyllide Oxidoreductase. *Nat. Struct. Biol.* **2003**, *10* (6), 491–492. https://doi.org/10.1038/nsb929.

(37) Townley, H. E.; Sessions, R. B.; Clarke, A. R.; Dafforn, T. R.; Griffiths, W. T.; Trevor Griffiths, W. Protochlorophyllide Oxidoreductase: A Homology Model Examined by Site-Directed Mutagenesis. *Proteins* **2001**, *44* (3), 329–335. https://doi.org/10.1002/prot.1098.

(38) Baker, M. E. Protochlorophyllide Reductase Is Homologous to Human Carbonyl Reductase and Pig 20β-Hydroxysteroid Dehydrogenase [2]. *Biochemical Journal*. 1994. https://doi.org/10.1042/bj3000605b.

(39) Silva, P. J.; Ramos, M. J. Computational Insights into the Photochemical Step of the Reaction Catalyzed by Protochlorophylide Oxidoreductase. *Int. J. Quantum Chem.* **2011**, *111* (7–8), 1472–1479. https://doi.org/10.1002/qua.22671.

(40) Zhang, S.; Heyes, D. J.; Feng, L.; Sun, W.; Johannissen, L. O.; Liu, H.; Levy, C. W.; Li, X.; Yang, J.; Yu, X.; et al. Structural Basis for Enzymatic Photocatalysis in Chlorophyll Biosynthesis. *Nature* **2019**, *574* (7780), 722–725. https://doi.org/10.1038/s41586-019-1685-2.

(41) Krieger, E.; Vriend, G. New Ways to Boost Molecular Dynamics Simulations. *J. Comput. Chem.* **2015**, n/a-n/a. https://doi.org/10.1002/jcc.23899.

(42) Jakalian, A.; Bush, B. L.; Jack, D. B.; Bayly, C. I.; I, A. C. A. M. Fast, Efficient Generation of High-Quality Atomic Charges. AM1-BCC Model: I. Method. *J. Comput. Chem.* **2000**, *21* (2), 132–146. https://doi.org/10.1002/(SICI)1096-987X(20000130)21:2<132::AID-JCC5>3.3.CO;2-G.

(43) Jakalian, A.; Jack, D. B.; Bayly, C. I. Fast, Efficient Generation of High-Quality Atomic Charges. AM1-BCC Model: II. Parameterization and Validation. *J. Comput. Chem.* **2002**, *23* (16), 1623–1641. https://doi.org/10.1002/jcc.10128.

(44) Duan, Y.; Wu, C.; Chowdhury, S.; Lee, M. C.; Xiong, G.; Zhang, W.; Yang, R.; Cieplak, P.; Luo, R.; Lee, T.; et al. A Point-Charge Force Field for Molecular Mechanics Simulations of Proteins Based on Condensed-Phase Quantum Mechanical Calculations. *J. Comput. Chem.* **2003**, *24* (16), 1999–2012. https://doi.org/10.1002/jcc.10349.

(45) Essmann, U.; Perera, L.; Berkowitz, M. L.; Darden, T.; Lee, H.; Pedersen, L. G. A Smooth Particle Mesh Ewald Method. *J. Chem. Phys.* **1995**, *103* (19), 8577–8593. https://doi.org/10.1063/1.470117.

(46) Berendsen, H. J. C.; Postma, J. P. M.; van Gunsteren, W. F.; DiNola, A.; Haak, J. R. Molecular Dynamics with Coupling to an External Bath. *J. Chem. Phys.* **1984**, *81* (8), 3684. https://doi.org/10.1063/1.448118.

(47) Trott, O.; Olson, A. J. AutoDock Vina: Improving the Speed and Accuracy of Docking with a New Scoring Function, Efficient Optimization, and Multithreading. *J. Comput. Chem.* **2010**, *31* (2), 455–461. https://doi.org/10.1002/jcc.21334.

(48) Kumar, S.; Bouzida, D.; Swendsen, R. H.; Kollman, P. A.; Rosenberg, J. M. The Weighted Histogram Analysis Method for Free Energy Calculations on Biomolecules: I. The Method. *J. Comp. Chem.* **1992**, *13* (8), 1011–1021. https://doi.org/http://dx.doi.org/10.1002/jcc.540130812.

(49) Grossfield, A. "WHAM: The Weighted Histogram Analysis Method." 2018.

(50) Adamo, C.; Barone, V. Toward Reliable Density Functional Methods without Adjustable Parameters: The PBE0 Model. *J. Chem. Phys.* **1999**, *110* (1999), 6158. https://doi.org/10.1063/1.478522.

(51) Ernzerhof, M.; Scuseria, G. E. Assessment of the Perdew–Burke–Ernzerhof Exchange-Correlation Functional. *J. Chem. Phys.* **1999**, *110* (11), 5029–5036. https://doi.org/10.1063/1.478401.

(52) Leang, S. S.; Zahariev, F.; Gordon, M. S. Benchmarking the Performance of Time-Dependent Density Functional Methods. *J. Chem. Phys.* **2012**, *136* (10). https://doi.org/10.1063/1.3689445.

(53) Baker, J.; Kessi, A.; Delley, B. The Generation and Use of Delocalized Internal Coordinates in Geometry Optimization. *J. Chem. Phys.* **1996**, *105*, 192–212. https://doi.org/10.1063/1.471864.

(54) Merrick, J. P.; Moran, D.; Radom, L. An Evaluation of Harmonic Vibrational Frequency Scale Factors. *J. Phys. Chem. A* **2007**, *111* (45), 11683–11700. https://doi.org/10.1021/jp073974n.

(55) Silva, P. J.; Ramos, M. J. A Comparative Density-Functional Study of the Reaction Mechanism of the O2-Dependent Coproporphyrinogen III Oxidase. *Bioorg. Med. Chem.* **2008**, *16* (6), 2726–2733. https://doi.org/10.1016/j.bmc.2008.01.008.

(56) Moser, C. C.; Dutton, P. L. Engineering Protein Structure for Electron Transfer Function in Photosynthetic Reaction Centers. *Biochim. Biophys. Acta - Bioenerg.* **1992**, *1101* (2), 171–176. https://doi.org/10.1016/0005-2728(92)90205-G.

(57) Tomasi, J.; Persico, M. Molecular Interactions in Solution: An Overview of Methods Based on Continuous Distributions of the Solvent. *Chem. Rev.* **1994**, *94* (7), 2027–2094. https://doi.org/10.1021/cr00031a013.

(58) Mennucci, B.; Tomasi, J. Continuum Solvation Models: A New Approach to the Problem of Solute's Charge Distribution and Cavity Boundaries. *J. Chem. Phys.* **1997**, *106* (12), 5151–5158. https://doi.org/10.1063/1.473558.

(59) Cossi, M.; Mennucci, B.; Pitarch, J.; Tomasi, J. Correction of Cavity-Induced Errors in Polarization Charges of Continuum Solvation Models. *J. Comput. Chem.* **1998**, *19* (8), 833–846. https://doi.org/10.1002/(sici)1096-987x(199806)19:8<833::aid-jcc3>3.0.co;2-q.

(60) Granovsky, A. A. Firefly 8.0.0. 2013, p http://classic.chem.msu.su/gran/gamess/index.html.

(61) Schmidt, M. W.; Baldridge, K. K.; Boatz, J. A.; Elbert, S. T.; Gordon, M. S.; Jensen, J. H.; Koseki, S.; Matsunaga, N.; Nguyen, K. A.; Su, S.; et al. General Atomic and Molecular Electronic Structure System. *J. Comput. Chem.* **1993**, *14* (11), 1347–1363. https://doi.org/10.1002/jcc.540141112.

(62) Bashford, D.; Gerwert, K. Electrostatic Calculations of the PKa Values of Ionizable Groups in Bacteriorhodopsin. *J. Mol. Biol.* **1992**, *224* (2), 473–486. https://doi.org/10.1016/0022-2836(92)91009-E.

(63) Maier, J. A.; Martinez, C.; Kasavajhala, K.; Wickstrom, L.; Hauser, K. E.; Simmerling, C. Ff14SB: Improving the Accuracy of Protein Side Chain and Backbone Parameters from Ff99SB. *J. Chem. Theory Comput.* **2015**, *11* (8), 3696–3713. https://doi.org/10.1021/acs.jctc.5b00255.

(64) Martel, P. J.; Soares, C. M.; Baptista, A. M.; Fuxreiter, M.; Náray-Szabó, G.; Louro, R. O.; Carrondo, M. A. Comparative Redox and PKa Calculations on Cytochrome C3 from Several Desulfovibrio Species Using Continuum Electrostatic Methods. *J. Biol. Inorg. Chem.* **1999**, *4* (1), 73–86.

(65) Antosiewicz, J.; McCammon, J. A.; Gilson, M. K. Prediction of PH-Dependent Properties of Proteins. *J. Mol. Biol.* **1994**, *238* (3), 415–436. https://doi.org/10.1006/jmbi.1994.1301.

(66) Baptista, A. M.; Martel, P. J.; Soares, C. M. Simulation of Electron-Proton Coupling with a Monte Carlo Method: Application to Cytochrome C3 Using Continuum Electrostatics. *Biophys. J.* **1999**, *76* (6), 2978–2998. https://doi.org/10.1016/S0006-3495(99)77452-7.

(67) Archipowa, N.; Kutta, R. J.; Heyes, D. J.; Scrutton, N. S. Stepwise Hydride Transfer in a Biological System: Insights into the Reaction Mechanism of the Light-Dependent Protochlorophyllide Oxidoreductase. *Angew. Chemie Int. Ed.* **2018**, *57* (10), 2682–2686. https://doi.org/10.1002/anie.201712729.

(68) Heyes, D. J.; Hardman, S. J. O.; Hedison, T. M.; Hoeven, R.; Greetham, G. M.; Towrie, M.; Scrutton, N. S. Excited-State Charge Separation in the Photochemical Mechanism of the Light-Driven Enzyme Protochlorophyllide Oxidoreductase. *Angew. Chem. Int. Ed. Engl.* **2014**, *54* (5), 1–5. https://doi.org/10.1002/anie.201409881.

(69) Page, C. C.; Moser, C. C.; Chen, X.; Dutton, P. L. Natural Engineering Principles of Electron Tunnelling in Biological Oxidation-Reduction. *Nature* **1999**, *402* (6757), 47–52. https://doi.org/10.1038/46972.

(70) Moser, C. C.; Page, C. C.; Farid, R.; Dutton, P. L. Biological Electron Transfer. *J. Bioenerg. Biomembr.* **1995**, *27* (3), 263–274.

(71) Menon, B. R. K. K.; Davison, P. A.; Hunter, C. N.; Scrutton, N. S.; Heyes, D. J. Mutagenesis Alters the Catalytic Mechanism of the Light-Driven Enzyme Protochlorophyllide Oxidoreductase. *J. Biol. Chem.* **2010**, *285* (3), 2113–2119. https://doi.org/10.1074/jbc.M109.071522.

(72) Heyes, D. J.; Ruban, A. V.; Hunter, C. N. Protochlorophyllide Oxidoreductase: "Dark" Reactions of a Light-Driven Enzyme. *Biochemistry* **2003**, *42* (2), 523–528. https://doi.org/10.1021/bi0268448.

(73) Belyaeva, O. B.; Litvin, F. F. Mechanisms of Phototransformation of Protochlorophyllide into Chlorophyllide. *Biochem. (Moscow).* **2014**, *79* (4), 337–348. https://doi.org/10.1134/S0006297914040038.

(74) Bublichenko, N. V., Umrikhina, A. V., Krasnovsky, A. A. [Free Radical Formation during the Photochemical Reactions of Protochlorophyll]. *Biofiz.* **1979**, *24*, 588–593.

(75) Belyaeva, O. B.; Timofeev, K. N.; Litvin, F. F. The Primary Reactions in the Protochlorophyll(Ide) Photoreduction as Investigated by Optical and ESR Spectroscopy. *Photosynth. Res.* **1988**, *15* (3), 247–256. https://doi.org/10.1007/BF00047356.

(76) Goldfeld, M. G.; Blumenfeld, L. A. Light-Dependent Paramagnetic Centers in the Photosynthesis of Higher Plants. *Bull. Magn. Reson.* **1979**, *1*, 66–112.

(77) Huber, M.; Fuhs, M. Frontier Orbitals of Porphyrin Electron Donors in - Partial Lifting of Orbital in Asymmetric by On. *Berichte der Bunsengesellschaft/Physical Chem. Chem. Phys.* **1996**, *100* (12), 2057–2064.

(78) Shimizu, D.; Osuka, A. Porphyrinoids as a Platform of Stable Radicals. *Chem. Sci.* **2018**, *9* (6), 1408–1423. https://doi.org/10.1039/c7sc05210c.